

# Concentric dual-loop RF coil for magnetic resonance imaging\*

R. Hernández

*Facultad de Ciencias-Universidad Nacional Autónoma de México,  
Ciudad Universitaria, México, D. F. 01000, México*

A. Rodríguez

*Departamento de Ingeniería Eléctrica, Universidad Autónoma Metropolitana-Iztapalapa,  
Av. San Rafael Atlixco 186, México, D. F., 09340, México,  
e-mail: arog@xanum.uam.mx*

P. Salgado

*American British Cowdray Medical Center, Mexico,  
D. F. 01120, México*

F.A. Barrios

*Instituto de Neurobiología, UNAM-Juriquilla, Queretaro,  
76230, México*

Recibido el 12 de julio de 2002; aceptado el 11 de diciembre de 2002

A surface coil for MRI consisted of two concentric loops was developed to produce brain images with a commercial MR imager. Prior to build the coil prototype, the magnetic field ( $B_1$ ) generated by the coil was numerically simulated. This field simulation is based on the Biot-Savart law for the circular- and square-shaped loop coils. From these theoretical results, we can appreciate an improvement on the  $B_1$  homogeneity. Comparison of experimental SNR for a single-loop and dual concentric figure coils show that the latter has better sensitivity and uniformity. Phantom and brain images were obtained on a 1.5 Tesla clinical imager, and showed a good image quality. These brain images when compared against images obtained with a circular-shaped coil exhibit a better capability of penetration. This receiver coil can generate high quality brain images. This coil design can be used in clinical imagers and is compatible with conventional imaging sequences and protocols.

*Keywords:* Magnetic resonance imaging; signal-to-noise ratio; surface RF coil; brain imaging.

Se desarrolló una antena superficial para ser usada en imagenología por resonancia magnética (IRM) para generar imágenes cerebrales con un sistema RM comercial. Previo a la construcción del prototipo, simulamos el campo magnético generado por la antena. La simulación del campo estuvo basada en la ley de Biot-Savart para los casos de las antenas de una sola espira de forma cuadrada y circular. De estos resultados se puede apreciar una mejora en la homogeneidad del campo. Se compararon los cocientes de señal a ruido (S/R) experimentales de una antena superficial de una sola espira y la antena concéntrica de dos espiras con geometrías distintas. Las gráficas mostraron una mejora en la sensibilidad y uniformidad para la antena de figuras concéntricas. Se obtuvieron imágenes de fantoma y cerebrales con un sistema clínico de resonancia magnética de 1.5 Teslas, mostrando una buena calidad de imagen. Este tipo de antenas pueden ser usadas en sistemas clínicos y con secuencias convencionales.

*Descriptores:* Imagenología por resonancia magnética; cociente señal a ruido; antena RF superficial; imagenología cerebral.

PACS: 87.57Ce; 87.61.Ff; 87.61.Lh

## 1. Introduction

### 1.1. Magnetic resonance imaging

This powerful imaging modality, commonly known as MRI, is a noninvasive tool to study both the anatomy and function of the human body. MRI belongs to a larger group of techniques which are based on the principles of the nuclear magnetic resonance (NMR). The NMR experiment described by Purcell [1] and Bloch [2] in 1946, can acquire a signal with no means to integrate the spatial information so as to generate an image. Since the word "nuclear" has an unfortunate connotation for the public, this imaging technique was called

MRI to avoid misconceptions. NMR was mainly used for spectroscopic analysis before the principles of MRI were introduced by Lauterbur [3] and Mansfield [4] independently in 1973. MRI can provide more information than other imaging modalities since MR signal are sensitive to several tissue parameters.

### 1.2. Radio frequency coil

Radio frequency coils, also known as RF resonators and RF probes, are key components in a magnetic resonance imager. They are called RF coils because they resonate at a specific radio frequency. RF coils in Magnetic Resonance Imaging

and Spectroscopy have two important functions: excitation of nuclear spins and detection of the resulting nuclear precession (signal). For the transmission case, the RF coil acts as a transducer which converts RF power into a transverse rotating RF magnetic field in the volume of interest. High efficiency in the transmission mode is associated to maximum magnetic field produced by the RF coil in the volume of interest for minimum RF power released to the region. In general, any coil can be operated in transmission mode or/and reception mode. When a RF coil is used as both a receiver and transmitter is then usually called a transceiver coil. Since a RF coil can be used for both reception and transmission of a MR signal, and to gain insight of the parameters involved in the design of a RF coil, the Principle of Reciprocity might be invoked [5]. This principle allows us to calculate the induced voltage and to deduce the field produced by a resonant circuit at any point.

MRI coils can be divided into major groups: a) surface coils. Single-loop and multiple-loop coils: the most popular is the circular-shaped coil [6] followed by the phased-array coils [7], however, other geometries and arrays have been proposed recently [8]; and b) volume coils. Some of them are: Helmholtz coil [9], saddle coil [10], high-pass and low-pass birdcage coils [11], and TEM resonator coils [12]. The birdcage coil has become the most widely used since is able to produce a very uniform  $B_1$  field over a large volume in the coil. A different type of coil has been recently introduced to meet the needs of the so called parallel imaging [13]. This kind of imaging sequence is able to parallel acquire signals coming from different coil elements to speed up the acquisition process. This imaging scheme is based on the coil sensitivity and it is denominated the SENSitivity Encoding technique (SENSE) [14].

Surface coils have become an important tool to produce high quality images and spectra in Magnetic Resonance Imaging and Spectroscopy. The idea of using a surface coil is intuitively attractive because, as is well known, the closer the coil is to the object being imaged, the more signal is expected. It is well known that surface antennae can produce a high  $SNR$  but poor uniformity. Therefore, an optimal design of a MRI coil should be able to generate a good homogeneity of the field and a high penetration capacity (good  $SNR$ ). Unfortunately, spatial uniformity and high-efficiency can not be optimised simultaneously. Increasing the homogeneity will increase the required power and decrease the  $SNR$ . The aim of this work is to develop a receiver coil with high sensitivity for brain imaging and spectroscopy applications. This coil is intended to be used in a clinical MR scanner. In order to clarify all the important aspects of the development of Radio Frequency coils in MRI, a brief review of the physical principles is presented. Then, a simple design motivated by the surface coil reported by Tomanek and co-workers [15] is built. Although this idea is not new, the previous work [16-21] did not use this approach to develop only-receiving surface coils.

In this paper a surface coil is proposed to generate brain images which is able to produce an improvement of the field

homogeneity and the penetration capacity. The present coil design was operated in the received-only mode. It consisted of two concentric single-loop coils of different size and geometry, namely a circular loop coil and a squared-shaped coil. A computer simulation of the magnetic field ( $B_1$ ) is presented for a particular size. Estimates of experimental  $SNR$  of the concentric loop coil and a single-loop coil obtained from phantom images are shown and compared. Phantom and brain images are presented to show the coil performance and compared against single-loop coil images.

## 2. Theory

When performing any MR Imaging experiment always appears an undesirable component that is uncorrelated to the signal. The Brownian motion of electrons in the receiver coil might be responsible and is the result of the coil resistance and temperature. A MRI experiment then involves the combination of two important parameters, signal and noise. This can be referred as the Signal-to-Noise Ratio:  $Signal/Noise$  or  $S/N$  or  $SNR$ . It has been previously stated that a good coil design should include a high  $SNR$ . This parameter is an accepted standard for measurement of quality in MRI studies [19]. The quality of the reconstructed images depends strongly on the  $SNR$  of the acquired signal. Modern imaging techniques often demand very high speed and spatial resolution, so that the highest possible  $SNR$  is still required to avoid poor image quality. The optimisation of the  $SNR$  is a major factor in the design of a RF receiver coil.

The MR signal is determined by the magnetic field generated by the coil. However, noise always accompanies a signal that is not solely due to the coil itself, but the human body as well. Unlike the  $SNR$  of the NMR experiment, in MRI the biological sample (patient) produces a resistance comparatively large since is a poor conductor, and contributes significantly in the noise figure induced in the coil.

To include the biological sample resistance, Hoult and Richard proposed a new  $SNR$  expression [5]:

$$SNR = \frac{Peak}{Signal} \propto \frac{\omega_0^2 B_1 i^{-1} V_{sample}}{R_{eff}}, \quad (1)$$

where  $\omega_0$  is the resonant frequency,  $V_{sample}$  is the voxel volume,  $B_1$  is the transverse linearly polarised magnetic field for unit current in the coil,  $R_{eff}$  is the effective resistance. The effective resistance includes contribution from the coil, electronics, and the sample being imaged (patient):

$$R_{eff} = R_{coil} + R_{sample} + R_{electronics}. \quad (2)$$

Since the electronics of a MR imager between 0.5 Tesla and 4 Teslas has improved significantly, imaging experiments carried out today on these systems it is possible to affirm that  $R_{eff}$  is approximately equal to  $R_{sample}$  (resistance caused by the patient).

The noise in any MRI experiment is basically thermal noise generated in the receiver coil and the sample and is de-

scribed by the Nyquist formula [20]:

$$R_{eff} = \sqrt{4\kappa T \Delta f R_{coil}}, \quad (3)$$

where  $\kappa$  represent the Boltzmann's constant,  $T$  is the sample temperature, the resistance,  $R_{coil}$  is used to represent the conductive losses of the coil itself as well as magnetic (eddy currents) and dielectric losses in the sample and surroundings structures. The noise is measured over a defined spectral bandwidth  $\Delta f$  in Hertz.

The *SNR* expression [Eq. (1)] also dictates the size and geometry of the RF coil to be developed. In particular, analytical expression of the  $R_{eff}$  and  $B_1$  for simple geometries have been developed by Wang and co-workers [21] who used the quasi-static approach to obtain a *SNR* formula. This produces accurate results for low field strengths ( $\leq 1$  Tesla) in which the wavelength is much larger than the body size. Schnell and collaborators [22] calculated the electromagnetic field of surface and volume coils by approximating the human body by a homogeneous half-space or cylinder depending on the type of coil to be used, to derive a general expression for the *SNR* in MRI. Ocali and Atalar [23] introduced another approach to calculate the intrinsic *SNR*, based on the assumption of a superposition of a large number of plane waves to obtain an expression for the electromagnetic field. The idea is to minimise the total power deposition while maintaining a constant right-hand circularly polarised component of the magnetic field at the point of interest. It is difficult to develop a simple relation between the imaging volume and the *SNR* of the associated RF coil, but it is still possible to see the increase of this parameter with the decrease of the coil's effective imaging volume as formulated in Eq. 1.

### 2.1. The RF coil as a coaxial transmission line

A medium to transmit the signal from the RF coil to the scanner is required, a coaxial (coax) or triaxial cable is usually used to connect the RF coil to the RF subsystem of the MR unit. The operation of the RF coil is not completely dependent upon the frequency response of the antenna itself but rather on the frequency characteristics of the transmission line-coil element combination. It also important to use a transmission line with a proper characteristic impedance to match the MR system, generally 50 ohms: the coaxial cable should then have a 50 ohms impedance as well. Another simple and practical technique that can be used to match the antenna to the transmission line is to use the  $\lambda/4$  transformer. This implies that the coil should be matched to the coax by using a  $\lambda/4$  piece of cable [24]. Because the signal travels through a coaxial cable: a RF attenuation by the cable is present, and although small is not negligible at some frequencies [25].

A RF coil attached to a coaxial cable forms a transmission line which is inherently unbalanced [26]. Because the inner and outer conductors are not coupled to the surface coil in the same way, they provide unbalance. Devices used to balance

this unbalanced system are denominated baluns (balance to unbalance).

### 2.2. Equivalent Circuit of a Surface RF coil

Viewing a RF coil as a magnetic energy storage device is a key to a good coil design. Surface coils are generally operated as resonant circuits. Then, an equivalent circuit can be formulated to study the parameters affecting the design of a RF coil. This is done in most applications to provide maximum power transfer between the MR system and the coil. In a resonant circuit, equal amounts of energy are stored in the electric and magnetic fields, with the energy exchanging repeatedly between the electric and magnetic fields. Electric fields with lossy dielectrics (patients) lead to increased resistance in the coil, the electric fields should be associated with the capacitors used for tuning and matching the coil rather than the stray electric field of the coil.

An easy way to represent a RF coil is using a resonant circuit composed of an inductor ( $L$ ), a resistance ( $R$ ) and a capacitance ( $C$ ). Consequently, using the Kirchoffs law for circuit in Fig. 1, it can be obtained that the resonant frequency is

$$\omega = \frac{1}{\sqrt{LC}}. \quad (4)$$

In practice, the resistance can not disappear totally so the current magnitude is never infinity. The current however would reach its maximum value at the resonant frequency.

### 2.3. The quality factor of a RLC circuit

To provide a quantitative way to measure the quality of the circuit, a quality factor,  $Q$  can be defined as the energy stored divided by the energy dissipated per period. However, to calculate the inductance and resistance of a coil is not an easy

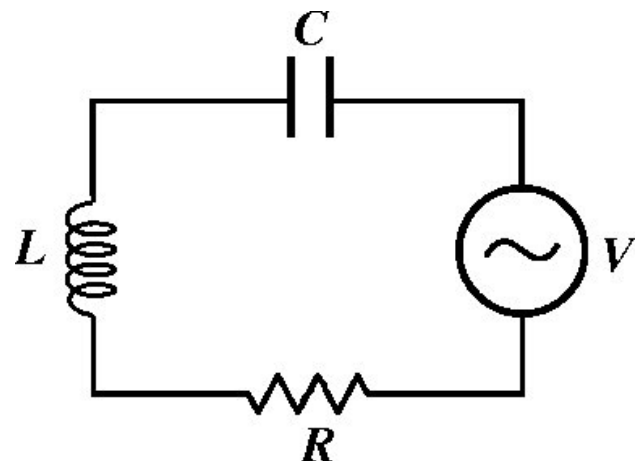


FIGURE 1. A typical representation of a RLC circuit.

task. The  $Q$  of a resonator can be expressed as:

$$Q = \frac{\text{maximum energy stored}}{\text{average energy dissipated per cycle}} = \frac{0.5I^2L}{\pi/\omega I^2 R_{coil}} = \frac{\omega L}{R_{coil}}. \quad (5)$$

From Eq. (5) it can be said that a high  $Q$  should have a small resistance. The higher the  $Q$ , the higher the ratio of flux density produced to power dissipated in the coil. Typical values for loaded coils ranges from order of magnitude of 10 to 100. The relative values of  $R_{coil}$  and  $R_{sample}$  in Eq. 2 can be determined by measuring the  $Q$  when the coil is empty and when it is loaded by a patient or a phantom. The best indicator of the coil sensitivity is the ratio

$$\frac{Q_{empty}}{Q_{loaded}} = \frac{R_{coil} + R_{sample}}{R_{coil}}, \quad (6)$$

provided the dielectric losses do not contribute to  $R_{sample}$  (patient). This ratio can be 5 times or more for a magnetic field strength of 1.5 Teslas, therefore coil losses contribute less than 11% of the observed noise value. Therefore, a good coil design should have a  $R_{sample} \gg R_{coil}$ .

A much simpler approach is to calculate  $Q$  according to the following expression [5]:

$$Q = \frac{\omega}{\Delta\omega}, \quad (7)$$

where  $\Delta\omega$  denotes the bandwidth, which can be measured easily with the aid of a network analyzer. The measured  $Q$  factor includes the contribution of the capacitor's resistance, and one must be aware that many capacitor manufacturers specify the  $Q$  of their products. High quality chip capacitors are then recommended to be used in the design of a MRI

coil, to avoid unwanted resistance contributions coming from these electronic components which can drastically affect the quality factor.

### 2.4. Coil homogeneity

MR images present intensity variations caused by the magnet magnetic field ( $B_0$ ), the RF coil field ( $B_1$ ) and eddy current compensation. In particular, the non-uniformity of the received field leads to unwanted variation in MR images. This effect is most pronounced with surface coils [27]. A number of quality tests have been reported to measure image uniformity [28]. This is normally carried out acquiring images under specific considerations. A crude manner to quantify this parameter can be obtained by plotting the pixel variation across an axial phantom image.

### 3. Methods

We designed and built a surface receiver coil with two concentric elements: a circular loop and a squared-shaped loop. In Fig. 2a an illustration of the coil prototype is shown. Prior to built this coil design, MATLAB programmes (V.6 Math-Works, Natick, MA) based on the Biot-Savart law were developed to visualise the magnetic field in the form of numerical simulations. All programmes were implemented on a 500 MHz Intel Pentium III PC.

The radius of the coil roughly matches the depth to which imaging is desired. Then, two copper substrate trips (width = 0.5 cm ) were used forming a squared-shaped coil with a side of 15.5 cm and a single-loop coil with a diameter of 14.0 cm. The square coil surrounded the circular coil to form a two-concentric figure coil with a separation of 0.5 cm from each other. Only tuning capacitors were soldered direc-

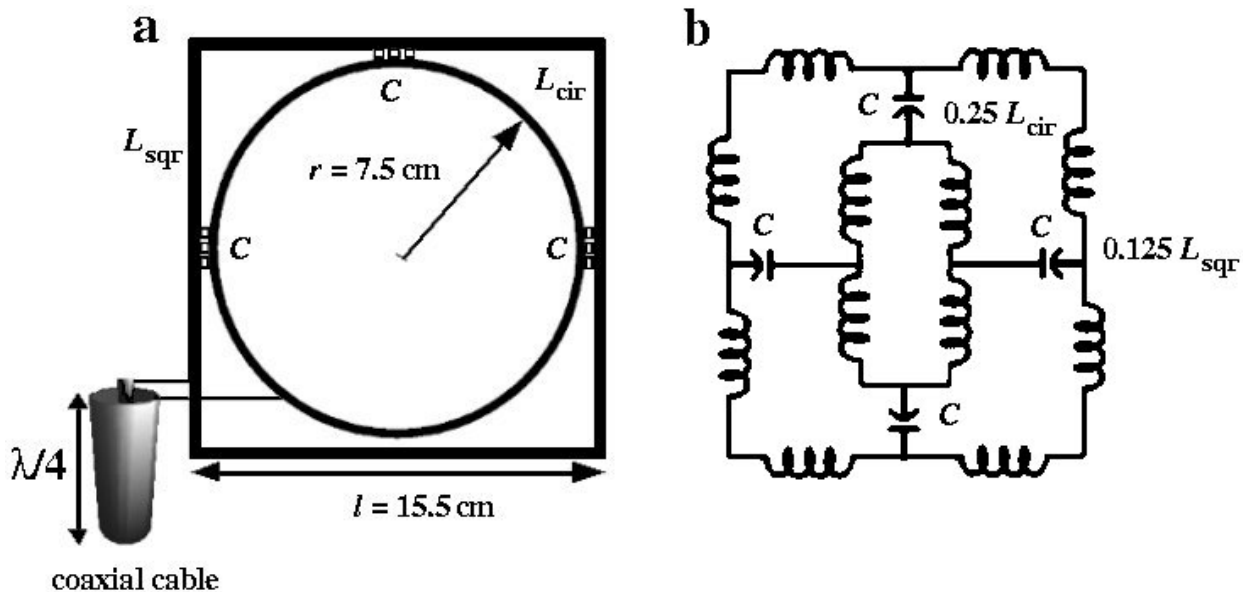


FIGURE 2. a) Schematic diagram of the dual concentric figure coil showing the prototype dimensions and localisation of the tuning capacitors, and b) equivalent electric circuit.

tly onto the surface of the two coil as follows: ceramics chip capacitors (American Technical Ceramics: series ATC 100 B non-magnetic) were placed between the middle point of each side of the squared-coil and the corresponding point on the circular coil. In order to balance the capacitance and reach the resonant frequency, chip capacitors were equally placed on the coils. The value of the capacitors were 15 pF and 75 pF ( $\pm 5\%$ ).

Since these coils are in the receive-only mode, a PIN diode (ECG 555A, Philips Electronics North America, Greeneville, TN) was placed parallel to the tuning capacitors between the central coil and the square coil. This allows us to avoid RF field concentrations at the coil conductor during transmission and to avoid coupling between the transmitter coil and receiver coil. To conduct the signal to the coil port of the MR imager, a 50 Ohm-coaxial cable (Model: 9223-low noise, Belden, Richmond, IN) was attached to the prototype and then matched and tuned to  $Z_0 = 50$  Ohm and  $\theta = 83.87$  MHz respectively, this frequency corresponds to a 1.5 Teslas MRI system.

An network analyzer (R3753 AH model, 5 Hz-500 MHz, Advantest Co, Tokyo, Japan) was used to measure the resonant frequencies as the return loss (S11). Then, the quality factor  $Q$  of the dual concentric figure coil was determined experimentally by measuring the resonant frequency of the coil divided by the 3-dB bandwidth, with quarter wavelength coaxial cable while placed on the top of a tap water filled phantom (35 cm in length and 7 cm in diameter) and was approximately 44, whereas for the unload case was 66. The coil prototype in Fig. 2a was tested on a 1.5 T imager (GE Signa LX equipped with V. 8.5, General Electric Medical Systems, Milwaukee, WI). A picture of the MRI systems of the Hospital ABC is shown in Fig. 3. Before any attempt is made to produce brain images of healthy volunteers, phantom images should be acquired to optimise the acquisition imaging protocol. Consequently, brain images of a healthy volunteer

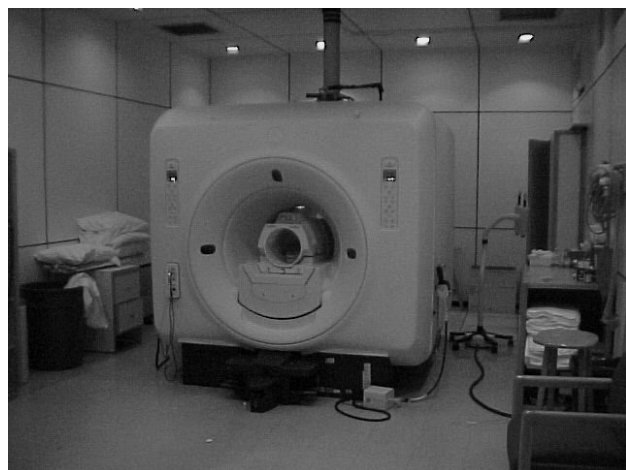


FIGURE 3. A picture of the clinical MR imager of the American British Cowdray Medical Center-Tacubaya, Mexico.

were acquired using the same parameters of the phantom imaging protocol. All imaging experiments were carried out under those circumstances normally found in the clinical environment, to ensure reproducibility of the imaging protocol.

#### 4. Results and discussion

A numerical simulation of the coil magnetic field ( $B_1$ ) was computed and depicted in Fig. 4. An improvement of the coil sensitivity can be observed from these contour maps. From the  $B_1$  field simulation, The loss return of the coil prototype is depicted in Fig. 5a. The RF antenna has a quality factor,  $Q = 64$  under loading conditions with a matching impedance of around 50 Ohms, see Fig. 5b. The following image acquisition parameters were used: TR/TE = 400 ms/7.5 ms, FOV = 18 cm, image size = 256x192, NEX = 5 for both phantom and brain imaging experiments. Phantom images in axial cuts were acquired and shown in Fig. 6. From these phantom images, a uniformity profile was computed to estimate the coil uniformity, see Fig. 7b. Phantom image data was used to compute the experimental profile of the SNR and compared it against the single-loop coil SNR roll-off. In both cases, phantom images were acquired with the same imaging protocol. A comparison of the SNR profiles is illustrated in Fig. 8. From these experimentally-acquired profiles, an improvement in the coil SNR can be appreciated. Figure 9 shows brain images in different orientations obtained with this coil prototype.

To simplify the design, no balun circuit was intentionally implemented for this coil. Tuning and matching were done by trial-and-error. It took a great deal of effort to reach the resonant frequency of the MR imager, as well as to get a matching figure around 50 Ohms. The MR scanner is equipped with a matching system that facilitates the use of RF coils not built by the same manufacturing company of the MR imager. Finally, there is no need to add a matching circuit to operate the scanner with this coil. No extra total resistance coming from the extra capacitors and inductors in the balun circuit was added, so a reduction of the resistance and an improvement of the image quality can be appreciated in the MR images themselves. The distribution of capacitance around the coil and mutual inductance require a better understanding. Coil mutual inductance can degrade the SNR reducing the penetration capacity of the surface coil, and an unbalanced distribution of energy can cause a higher matching capacitance that unable to tune the structure to the desired resonant frequency. Both parameters can be studied through the analysis of the properties of the equivalent circuit in Fig. 1b, and a circuit simulator such as SPICE (29) which is able to simulate the loss return response in a reliable fashion. Additionally, these results might be of some help to avoid the used of baluns or other matching circuits, and replacing the trial-and-error scheme.

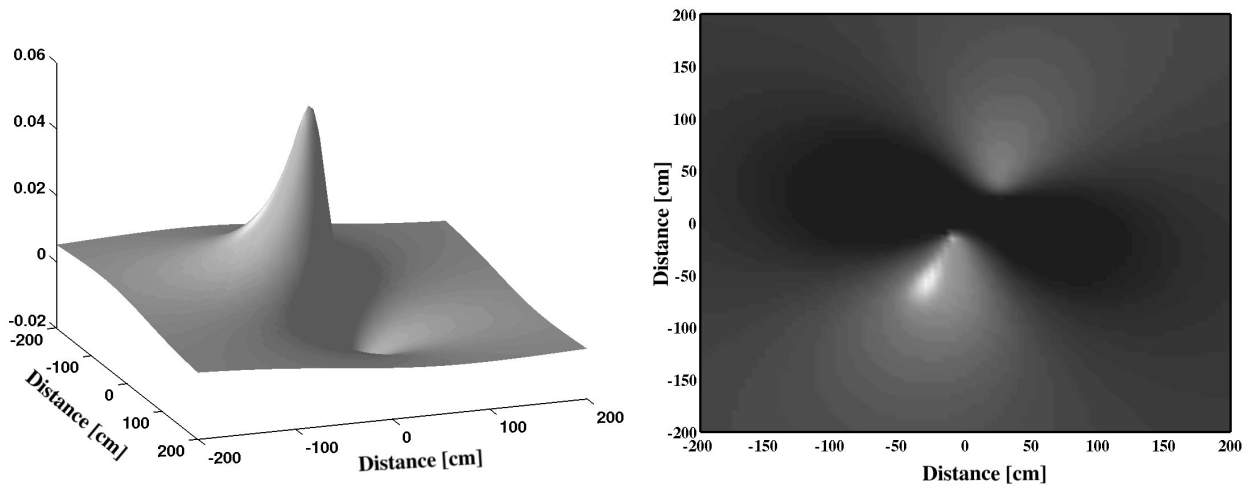


FIGURE 4. Two different views of the numerical simulation of magnetic field generated by the dual concentric figure coil.

Phantom images in Fig. 6, exhibit a high image quality since details in the General Electric cylindrical phantom can

be easily observed. These images also show an good uniformity and penetration for brain imaging. This coil prototype quantitatively shows a better performance than the single-loop coil. From the purely qualitative comparison of images in Fig. 6, we can appreciate an betterment in the image SNR. A more formal analysis is required to quantitatively assess the SNR and field uniformity and compare to other common surface coils. The experimental evidence acquired with the phantom imaging experiments (Figs. 6-8) shows a better SNR when compared against a single-loop coil.

Coronal and transversal brain images of Fig. 9 show a nonuniform reception profile in the central region. This a

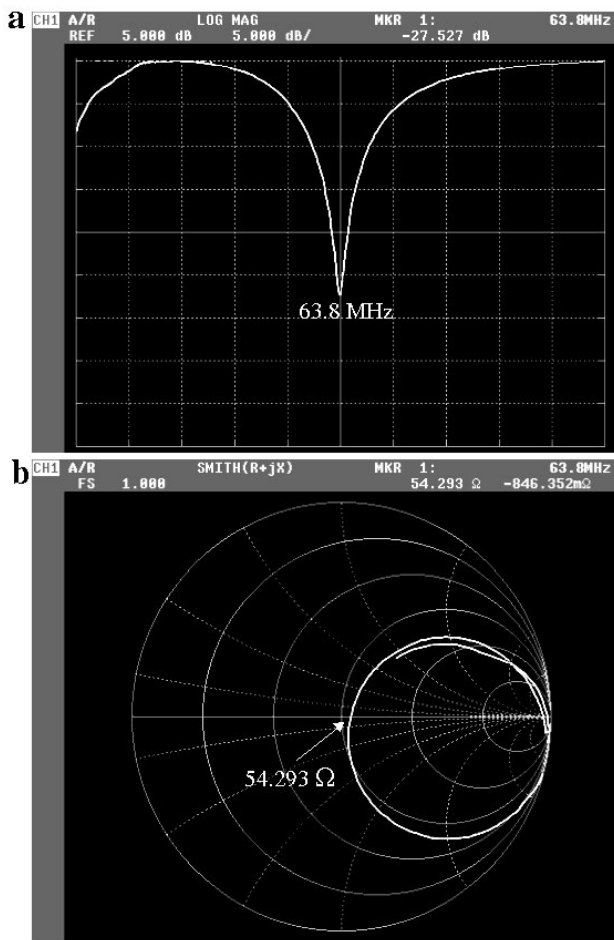


FIGURE 5. Illustrations of the coil characterisation obtained with the aid of a network analyzer for both tuning and matching: a) estimation of loss return measured with a network analyzer, and b) Smith chart of the nearly 50 ohm-matching of the prototype.

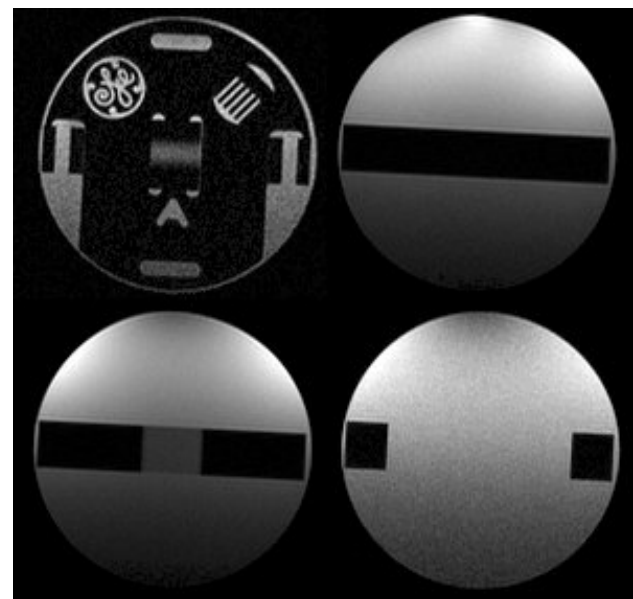


FIGURE 6. Phantom images obtained from a General Electric phantom in axial cuts at various position along the cylindrical phantom. These images show a high uniformity and very good spatial resolution in all four cases.

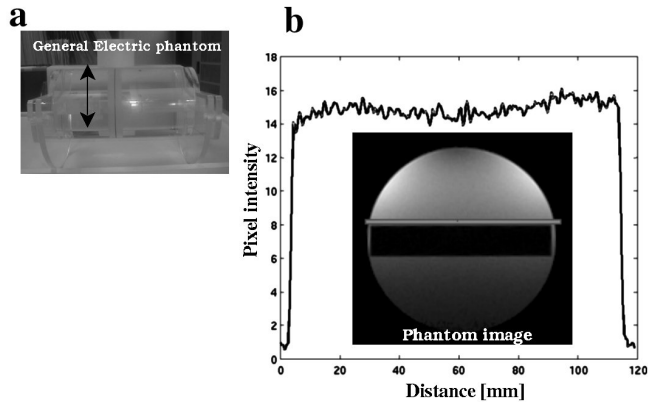


FIGURE 7. a) Picture of a General Electric cylindrical phantom (Model 2131027-2, NIC12 +H<sub>2</sub>O, weight = 4.43 kg): the arrow shows the location where the image was acquired. b) Plot of pixel intensity variation versus phantom diameter. Uniformity data was taken across the phantom as indicated in the image below.

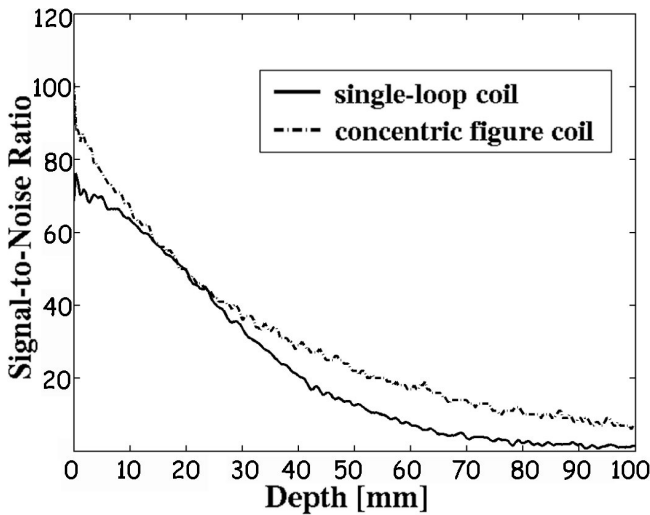


FIGURE 8. Comparison of experimental SNR roll-offs of a single-loop coil (radius = 10 cm) and the dual concentric figure coil. Both profiles were computed from phantom images acquired with the same imaging protocol as for the brain imaging experiments.

very similar artefact as those generated by the phased-array coils, and it can be corrected by applying some image intensity correction method as the edge-filled low-pass image correction algorithm. However, brain images obtained with this coil prototype show a good image quality. However, after correcting the nonuniform profile, image quality can be enhanced so brain images can be used for clinical and diagnostic purposes. A comparison of image quality can be observed in Fig. 10, for images acquired with a single-loop coil and the concentric dual-loop coil.

This surface coil can be used in a clinical MR scanner in a simple manner and no extra care should be taken. Imaging experiments showed that this coil has a full compatibility with imaging schemes such as Spin and Gradient Echo sequences. Majority of imagers in the world are equipped with at least one of this pulse sequences, and built on the same

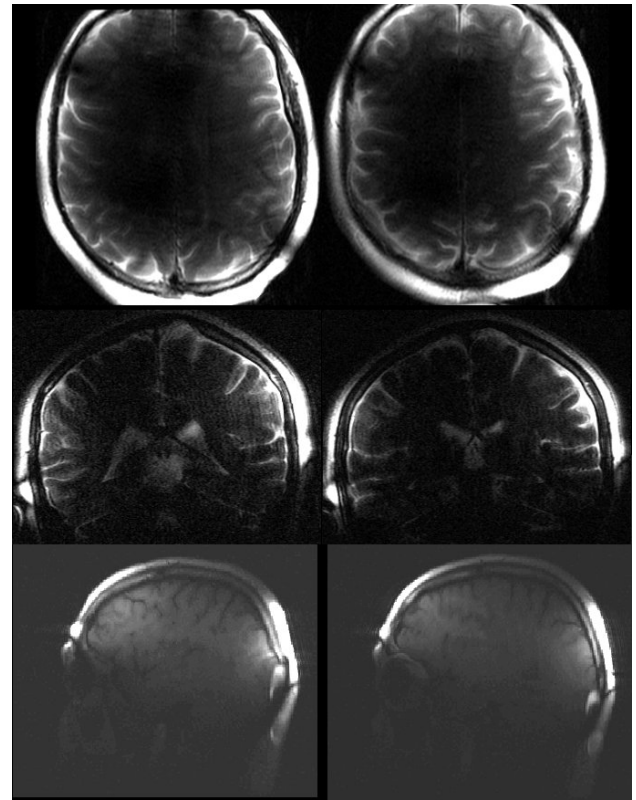


FIGURE 9. Brain images acquired with the dual concentric figure coil in three directions and the same acquisition parameters.

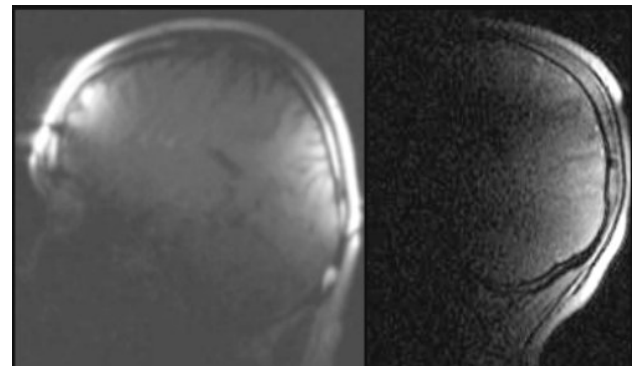


FIGURE 10. Comparison of brain images using the same imaging acquisition protocol a) concentric loop coil, and b) single-loop coil.

principles. This implies that this coil design can be used in any commercial scanner regardless the manufacturing company. Further improvements in the coil should include the use of different coil geometries and sizes. This may further improve the coil array uniformity and the penetration capability.

### 5. Conclusion

In summary, a surface coil with two different concentric loops was designed and built for brain imaging. It has been

demonstrated that this coil can be used in a clinical imager. The SNR of dual concentric figure coil is a qualitatively higher than a single-loop coil one with similar coil dimensions. This type of coil can improve the sensitivity as well as uniformity of an image. Mutual inductance degrades the image quality so further work is required to quantify this unwanted effect. Clinical MR scanner compatibility allows these RF receiver coils to be used with conventional pulse sequences and imaging protocols. These arrays have an inexpensive and flexible design that enables them to be used for various imaging applications including the heart, spine, and pelvis.

## Acknowledgement

We would like to express our gratitude to the American Hospital Cowdray Medical Center for allowing us to carry out all the imaging experiments. We thank General Electric Sistemas Medicos and Schering Mexicana for the support of this research. FAB gratefully acknowledges the National Council of Science and Technology of Mexico (CONACYT) for the research grant: R 31162 A.

- 
- \*. This work was presented in part at the 6th Mexican Symposium on Medical Physics, CINVESTAV-Sur, Mexico, D.F., 2002.
1. E.M. Purcell, H.C. Torrey, and R.V. Pound, *Phys. Rev.* **69** (1946) 37.
  2. F. Bloch, *Phys. Rev.* **70** (1946) 460.
  3. P.C. Lauterbur, *Nature* **242** (1973) 190.
  4. P. Mansfield and P.K. Grannell, *J. Phys. C: Solid State Phys* **6** (1973) L422.
  5. D.I. Hoult and R.E. Richards, *J. Magn. Reson.* **24** (1976) 71.
  6. J.J.H. Ackerman, T.H. Grove, G.G. Wong, D.G. Gadian, and G.K. Radda, *Nature* **283** (1980) 167.
  7. B. Roemer, W.A. Edelstein, C.E. Hayes, S.P. Souza, and O.M. Muller, *Magn. Reson. Med.* **16** (1990) 192.
  8. S. Hidalgo, A.O. Rodriguez, R. Rojas, J. Sanchez, G. Reynoso, F. Barrios, Proc 9th Inter. Soc. Magn. Reson. Med. (Glasgow, Scotland, 2001) p. 1112.
  9. C-N. Chen, and D.I. Hoult, *Biomedical Magnetic Resonance Technology*, (Adam Hilger-IOP Publishing, Bristol, 1989).
  10. J. Jin, *Electromagnetic Analysis and Design*, (CRC Press, Boca Raton, 1999).
  11. C.E. Hayes, W.A. Edelstein, J.F. Schenk, O.M. Mueller, and M.E. Eash, *J. Magn. Reson.* **63** (1985) 622.
  12. P. Roschmann, *Med. Phys.* **14** (1987) 922.
  13. M. Weiger, K.P. Pruessmann, C. Leussler, P. Roschmann, and P. Boesiger, *Magn. Reson. Med.* **45** (2001) 495.
  14. K.P. Pruessmann, M. Weiger, M.B. Scheidegger, and P. Boesiger, *Magn. Reson. Med.* **42** (1999) 952.
  15. B. Tomanek, L. Ryner, D.I. Hoult, P. Kozlowski, and J.K. Saunders, *Magn. Reson. Imaging* **15** (1997) 1199.
  16. J.H. Battocletti *et al.*, *Med. Biol. Eng. Comput.* **17** (1979) 183.
  17. M.R. Bendall, *Chem. Phys. Lett.* **99** (1983) 310.
  18. P. Styles, M.B. Smith, R.W. Briggs, and G.K. Radda, *J. Magn. Reson.* **62** (1985) 397.
  19. T.W. Redpath, *Br. J. Radiol.* **71** (1998) 704.
  20. D.I. Hoult, *Prog. NMR Spec.* **12** (1978) 41.
  21. J. Wang, A. Rezkowski, and J. Dickas, *IEEE Trans. Biomed. Eng.* **42** (1995) 908.
  22. W. Schnell, W. Renz, M. Vester, and H. Ermert, *IEEE Trans. Ant. Prop.* **48** (2000) 418.
  23. O. Ocali and E. Atalar, *Magn. Reson. Med.* **39** (1998) 462.
  24. D.M. Pozar, *Microwave Engineering* (Addison-Wesley Publishing Co, 1990).
  25. D.E. MacLaughlin, *Rev. Sci. Instrum.* **60** (1989) 3242.
  26. C.A. Balanis, *Antenna Theory: Analysis and Design* (2nd Ed, John Wiley & Sons, New York, 1997).
  27. G.J. Barker, A. Simmons, S.R. Arridge, and P.S. Tofts, *Br. J. Radiol.* **71** (1998) 59.
  28. R.I. Dixon (editor), *MRI: Acceptance testing and quality control. The role of the clinical medical physicist*, Proceedings of an AAPM Symposium (Medical Physics Publishing Co, Madison, 1988).
  29. M.H. Rashid, *Spice for Circuits and Electronics: Using PSPICE*, (Prentice-Hall, Englewood Cliffs, 1990).